

Differentiable Bayesian Structure Learning with Acyclicity Assurance

Quang-Duy Tran, Phuoc Nguyen, Bao Duong, Thin Nguyen
Applied Artificial Intelligence Institute (A²I²), Deakin University, Geelong, Australia
 {q.tran, phuoc.nguyen, duongng, thin.nguyen}@deakin.edu.au

Abstract—Score-based approaches in the structure learning task are thriving because of their scalability. Continuous relaxation has been the key reason for this advancement. Despite achieving promising outcomes, most of these methods are still struggling to ensure that the graphs generated from the latent space are acyclic by minimizing a defined score. There has also been another trend of permutation-based approaches, which concern the search for the topological ordering of the variables in the directed acyclic graph in order to limit the search space of the graph. In this study, we propose an alternative approach for strictly constraining the acyclicity of the graphs with an integration of the knowledge from the topological orderings. Our approach can reduce inference complexity while ensuring the structures of the generated graphs to be acyclic. Our empirical experiments with simulated and real-world data show that our approach can outperform related Bayesian score-based approaches.

Index Terms—Bayesian structure learning, acyclicity constraint, topological ordering.

I. INTRODUCTION

Structure learning aims to uncover the underlying directed acyclic graphs (DAGs) from observational data that can represent statistical or causal relationships between variables. The structure learning task has many applications in biology [36], economics [21], and interpretable machine learning [30]. Correspondingly, it is gaining scientific interest in various domains such as computer science, statistics, and bioinformatics [41]. One challenge of traditional structure learning methods such as GES [6] is the combinatorial search space of possible DAGs [7]. NO-TEARS [46] proposes a solution for this challenge by relaxing the formulation of the learning task in a continuous space and employs continuous optimization techniques. However, with the continuous representations, another challenge also arises which is the acyclicity constraint of the graphs.

In most continuous score-based methods [46], [47], [25], [26], the constraints of graph acyclicity are defined in a form of a penalizing score and minimizing the score will also minimize the cyclicity of the graphs. This type of approach requires a large number of running steps with complex penalization weight scheduling to ensure the correctness of the constraint, which varies greatly depending on settings. This lack of certainty will affect the quality and restrict the applicability of the learned structures. Another approach is to embed the constraint acyclicity in the generative model of the graphs such as in [8] by utilizing weighted adjacency matrices that can be decomposed into the combinations of a permutation matrix

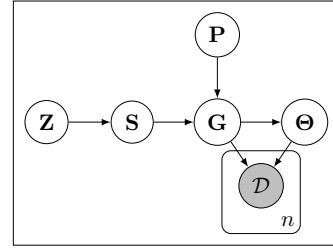


Fig. 1. The proposed generative model of the Bayesian networks in Topological Ordering in Differentiable Bayesian Structure Learning with Acyclicity Assurance (TOBAC). S , which has a strictly upper triangular form, is the adjacency matrix of the DAG when the topological ordering of the variables is correct. This matrix is generated from a latent variable Z . For each instance of the permutation matrix P , the rows and columns in S can be permuted to generate an isomorphic graph G . The variable Θ defines the parameters of the local conditional distributions of the nodes given their parents in G . The observational data \mathcal{D} consisting of n observations is assumed to be generated from this generative model.

and a strictly lower triangular matrix. Our study is inspired by this approach by using a direct constraint in the generation process instead of a post-hoc penalizing score.

There is a parallel branch of permutation-based causal discovery approaches whose methods allow us to find the topological ordering in polynomial time [5], [14], [35], [37], which can provide beneficial information. Inspired by these approaches, we propose a framework, Topological Ordering in Differentiable Bayesian Structure Learning with Acylicity Assurance (TOBAC), to greatly reduce the difficulty of the acyclicity-constraining task. Conditional inference is performed in this framework with the condition being the prior knowledge provided from the topological orderings. Our work is based on the independent factorization property of a DAG's adjacency matrix into a permutation matrix P and a strictly upper triangular matrix S which represents the adjacency matrix when the ordering is correct. The factorization $p(G, S, P) = p(S)p(P)p(G | S, P)$ allows us to infer P and S independently. Especially, decoupling these enables us to apply recent advances in learning of topological ordering and probabilistic model inference techniques. For each case of the permutation matrix P , we can infer the DAG's strictly upper triangular matrix S and compute the adjacency of an isomorphic DAG with $G = PSP^T$. In order to infer this DAG G , we choose the recent graph inference approach in this field, DiBS [25], as ours inference engine for S . We run experiments on synthetic data and a real flow cytometry

dataset [36] in linear and nonlinear Gaussian settings. The proposed constraint in the structure approach shows better DAG predictions and achieves better performance compared to other approaches.

Contributions. The main contributions of this study are summarized as follows

- 1) We address the limitations of post-hoc acyclicity constraint scores by strictly constraining the generative structure of the graphs. By utilizing the permutation-based decomposition of the adjacency matrix, we can strictly guarantee the acyclicity constraint in Bayesian network.
- 2) We introduce TOBAC, a framework for independently inferring and conditioning on the topological ordering. Our inference process guarantees the acyclicity of inferred graphs as well as reduces the inference complexity of the adjacency matrices.
- 3) We demonstrate the effectiveness of TOBAC in comparison with related state-of-the-art Bayesian score-based methods on both synthetic and real-world. Our approach obtains better performance on synthetic linear and nonlinear Gaussian data and on the real flow cytometry dataset.

II. RELATED WORKS

a) Bayesian structure learning methods: Most structure learning approaches can be categorized by their learning objectives into two main categories. The majority of methods [5], [6], [22], [31], [35], [37], [46], [47] fall into the first category where each method aims to recover a point estimate or its Markov equivalence class. In the other category, which is called Bayesian structure learning, the methods [8], [9], [13], [20], [25], [26], [28] aim to learn the posterior distribution over the DAGs given the observational data, i.e., $p(G | \mathcal{D})$. These methods can quantify the epistemic uncertainty in cases such as limited number of sample size or non-identifiable models in causal discovery. Previous approaches to learning the posterior distribution are diverse for example, using Markov chain Monte Carlo (MCMC) [28], bootstrapping [13] with PC [40] and GES [6], and exact methods with dynamic programming [20]. Recent Bayesian structure learning approaches use more advanced methods such as variational inference [8], [25], [26] or Generative Flow Networks (GFlowNets) [2], [9], [32], [10].

b) Permutation-based methods: Searching over the space of the permutations of the variables is significantly faster than searching over the space of possible DAGs. When the correct topological ordering of a DAG is found, a skeleton containing possible relations can be constructed and the DAG can be easily retrieved from this skeleton using the available conditional independence tests [4], [34], [39], [43], [42]. There has been many approaches for both linear [5], [45] and nonlinear additive noise models [14], [35], [37], [31]. EqVar [5] learns the topological orderings with the assumption of equal variances. NPVar [14] extends the work of EqVar by replacing the error variances with the corresponding residual

variances and modeling using the nonparametric setting. Both of these methods iteratively find the root nodes to the leaf nodes of the causal DAG. Alternatively, SCORE [35] finds the leaves from a score estimated to match the gradient of the log probability distribution of the variables.

c) Score-based methods: For fully observed data, early method such as GES [6] uses greedy search to efficiently search for the causal order in the permutation space by maximizing a score function. Recent developments efficiently search for the sparsest permutation, as in the Sparsest Permutation algorithm [34] and Greedy Sparsest Permutation algorithm [39], over the vertices of a permutohedron representing the space of permutations of DAGs, and reduce the search space by contracting the vertices corresponding to the same DAG [39]. These methods are also adapted for interventional data in [43], [42]. Another recent approach in this category is the group of DAG-GFlowNet [9], [32], [10] methods, which utilizes GFlowNet to search over the states of DAGs and can approximate the posterior distribution using both observational and interventional data.

d) Continuous score-based methods: Structure learning approaches with continuous relaxation [47], [22], [44], [8], [25], [26] is developing rapidly since NO-TEARS [46] was introduced. A continuous search space allows us to optimize or infer using gradient-based approaches to avoid search over the large space of discrete DAGs. Bayesian inference with variational inference is one category of the gradient-based approaches used in the latest frameworks [8], [25], [26]. BCD Nets [8] decomposes the weighted adjacency matrix to a permutation matrix and a strictly lower triangular matrix, and infers the probabilities of these matrices using the evidence lower bound (ELBO) of the variational inference problem. DiBS [25] models the probabilities of the edges using a bilinear generative model from the latent space and infers the posterior using Stein variational gradient descent.

e) Topological ordering in continuous score-based methods: Topological orderings appear variously in these continuous approaches. These recent advances use probabilistic models based on neural networks for (1) estimating the topological order directly as in BCD Nets [8] in the form of a permutation matrix, or (2) sidestepping the topological order estimation by including an auxiliary DAG constraint [46], [47], [23] or regularization [44], [22], [25], [26] instead. Our framework belongs to the former category, but we avoid the complexity in the joint inference of the permutation matrix and the graph. In this study, we design an acyclicity-ensuring conditional inference process with the topological ordering as a condition. With this process setting, we can effectively integrate the knowledge from the topological ordering into the inference to achieve higher inference efficiency.

III. TOBAC: TOPOLOGICAL ORDERING IN DIFFERENTIABLE BAYESIAN STRUCTURE LEARNING WITH ACYCLICITY ASSURANCE

A. Acyclicity Assurance via Decomposition of Adjacency Matrix

To analyze the decomposition of the adjacency matrix of a directed acyclic graph (DAG), we need to start from the topological orderings. A topological ordering (or, in short, an ordering) is a topological sort of the variables in a DAG. Let $\pi = [\pi_1, \pi_2, \dots, \pi_d]$ be the corresponding ordering of the variables $\mathbf{X} = [X_1, X_2, \dots, X_d]$, and $\pi_i < \pi_j$ means that $X_i \in nd(X_j)$ where $nd(X_j)$ is the set containing the non-descendants of X_j . We consider the canonical case where the ordering of the variables is already correct, i.e., $\pi^* = [\pi_i^* = i, \forall i]$. In this case, because every variable X_i is a non-descendant of X_j if $i < j$, the adjacency matrix \mathbf{G} of the DAG will become a strictly upper triangular matrix $\mathbf{S} \in \{0, 1\}^{d \times d}$.

In order to generalize to any ordering, we use a permutation matrix \mathbf{P} that transforms the ordering π to π^* as

$$P_{i,j} = \begin{cases} 1 & \text{if } i = \pi_j, \\ 0 & \text{otherwise.} \end{cases} \quad (1)$$

With this permutation matrix, we can always generate the adjacency matrix of an isomorphic DAG by

$$\mathbf{G} = \mathbf{PSP}^\top. \quad (2)$$

This formulation shifts the corresponding rows and columns in \mathbf{G} from the canonical ordering π^* to the ordering π . As the canonical adjacency matrix is acyclic, the derived graphs will always satisfy acyclicity. By employing this decomposition in the generative process, the acyclicity of the inferred graphs will always be satisfied.

B. Representing the Canonical Adjacency Matrix in a Latent Space

With every permutation matrix \mathbf{P} , we only need to find the equivalent canonical adjacency matrix \mathbf{S} . Following the DiBS approach in [25], this matrix is sampled from a latent variable \mathbf{Z} consisting of two embedding matrices $\mathbf{U} = [\mathbf{u}_1, \mathbf{u}_2, \dots, \mathbf{u}_{d-1}]$, $\mathbf{u}_i \in \mathbb{R}^k$ and $\mathbf{V} = [\mathbf{v}_1, \mathbf{v}_2, \dots, \mathbf{v}_{d-1}]$, $\mathbf{v}_j \in \mathbb{R}^k$. Due to the nature of strictly upper triangular matrices, only $d-1$ vectors in each embedding are needed to construct \mathbf{S} instead of d vectors as in DiBS. Following this configuration, the dimension k of the latent vectors is chosen to be greater or equal to $d-1$ to ensure that the generated graphs are not constrained in rank. We represent the probabilities of values in \mathbf{S} as follows

$$\mathbf{S}_\alpha(\mathbf{Z})_{i,j} := p_\alpha(S_{i,j} = 1 \mid \mathbf{u}_i, \mathbf{v}_{j-1}) \quad (3)$$

$$= \begin{cases} \sigma_\alpha(\mathbf{u}_i^\top \mathbf{v}_{j-1}) & \text{if } j > i, \\ 0 & \text{otherwise;} \end{cases} \quad (4)$$

where $\sigma_\alpha(x) = 1/(1 + \exp(-\alpha x))$ and the term α will be increased each step to make the sigmoid function $\sigma_\alpha(x)$

converge to the Heaviside step function $\mathbb{1}[x > 0]$. As $\alpha \rightarrow \infty$, the converged generated \mathbf{S}_∞ will become

$$\mathbf{S}_\infty(\mathbf{Z})_{i,j} := \begin{cases} \mathbb{1}[\mathbf{u}_i^\top \mathbf{v}_{j-1} > 0] & \text{if } j > i, \\ 0 & \text{otherwise.} \end{cases} \quad (5)$$

The probability of the edges in the adjacency matrix \mathbf{G} given the latent variable \mathbf{Z} and the permutation matrix \mathbf{P} can be computed by

$$\begin{aligned} p_\alpha(G_{i,j} = 1 \mid \mathbf{Z}, \mathbf{P}) \\ := \sum_{a=1}^d \sum_{b=1}^d P_{i,b} p_\alpha(S_{b,a} = 1 \mid \mathbf{Z}) P_{a,j}^\top \end{aligned} \quad (6)$$

C. Estimating the Latent Variable using Bayesian Inference

In order to estimate the latent variable \mathbf{Z} , extending the approach from [25], we first consider the generative model given in Figure 1. In this figure, a Bayesian network consists of a pair of variables (\mathbf{G}, Θ) where Θ defines the parameters of the local conditional distributions at each variable given its parents in the DAG. This generative model are assumed to generate the observational data \mathcal{D} containing n observations.

Given a permutation matrix \mathbf{P} , the generative model conditioned on \mathbf{P} can be factorized as

$$\begin{aligned} p(\mathbf{Z}, \mathbf{S}, \mathbf{G}, \Theta, \mathcal{D} \mid \mathbf{P}) \\ = p(\mathbf{Z}) p(\mathbf{S} \mid \mathbf{Z}, \mathbf{P}) p(\mathbf{G} \mid \mathbf{S}, \mathbf{P}) p(\Theta \mid \mathbf{G}) p(\mathcal{D} \mid \mathbf{G}, \Theta). \end{aligned} \quad (7)$$

For any function $f(\mathbf{G}, \Theta)$ of interest, we can compute its expectation from the distribution $p(\mathbf{G}, \Theta \mid \mathcal{D}, \mathbf{P})$ by inferring $p(\mathbf{Z}, \Theta \mid \mathcal{D}, \mathbf{P})$ with the following formula

$$\begin{aligned} \mathbb{E}_{p(\mathbf{G}, \Theta \mid \mathcal{D}, \mathbf{P})} [f(\mathbf{G}, \Theta)] \\ = \mathbb{E}_{p(\mathbf{Z}, \Theta \mid \mathcal{D}, \mathbf{P})} \left[\frac{\mathbb{E}_{p(\mathbf{G} \mid \mathbf{Z}, \mathbf{P})} [f(\mathbf{G}, \Theta) p(\Theta, \mathcal{D} \mid \mathbf{G})]}{\mathbb{E}_{p(\mathbf{G} \mid \mathbf{Z}, \mathbf{P})} [p(\Theta, \mathcal{D} \mid \mathbf{G})]} \right], \end{aligned} \quad (8)$$

where $p(\Theta, \mathcal{D} \mid \mathbf{G}) = p(\Theta \mid \mathbf{G}) p(\mathcal{D} \mid \mathbf{G}, \Theta)$ and $p(\mathbf{G} \mid \mathbf{Z}, \mathbf{P})$ is computed using a graph prior (e.g., Erdős–Rényi [12] or scale-free [1]) with the soft graph in Equation (6). The function $f(\mathbf{G}, \Theta)$ in Equation (8) acts as a placeholder for $p(\mathcal{D} \mid \mathbf{G}, \Theta)$ in this study or any other functions depending on the setting of each structure learning task. The distributions of the parameters $p(\Theta \mid \mathbf{G})$ and the data $p(\mathcal{D} \mid \mathbf{G}, \Theta)$ are chosen differently for the linear and nonlinear Gaussian models. In the linear Gaussian model, the log probability of the parameters given the graph is

$$\log p(\Theta \mid \mathbf{G}) = \sum_{i,j} G_{i,j} \log \mathcal{N}(\theta_{i,j}; \mu_e, \sigma_e^2), \quad (9)$$

where μ_e and σ_e are the mean and standard deviation of the Gaussian edge weights, and the log likelihood is as follows

$$\log p(\mathcal{D} \mid \mathbf{G}, \Theta) = \sum_{i=1}^d \log \mathcal{N}(X_i; \theta_i^\top \mathbf{X}_{\text{pa}(i)}, \sigma_{obs}^2), \quad (10)$$

where σ_{obs} is the standard deviation of the additive observation noise at each node. In the nonlinear Gaussian model, we follow [47], [25] by using the feed-forward neural networks (FFNs) denoted by $\text{FFN}(\cdot; \Theta) : \mathbb{R}^d \rightarrow \mathbb{R}$ to represent the relation of

the variables with their parents (i.e., $f_i(\mathbf{X}_{pa(i)})$ for each X_i). For each variable X_i , the output is computed as

$$\begin{aligned} & \text{FFN}(\mathbf{x}; \Theta^{(i)}) \\ & := \Theta^{(i,L)} f_a \left(\dots \Theta^{(i,2)} f_a \left(\Theta^{(i,1)} \mathbf{x} + \theta_b^{(i,1)} \right) + \theta_b^{(i,2)} \dots \right) \\ & \quad + \theta_b^{(i,L)}, \end{aligned} \quad (11)$$

where $\Theta^{(i,l)} \in \mathbb{R}^{d_l \times d_{l-1}}$ is the weight matrix, $\theta_b^{(i,l)} \in \mathbb{R}^{d_l}$ is the bias vector, and f_a is the activation function. From the model in this setting, the log probability of the parameters is

$$\begin{aligned} \log p(\Theta | \mathbf{G}) &= \sum_{i=1}^d \left(\sum_{a=1}^{d_1} \left(\log \mathcal{N} \left(\left(\theta_b^{(i,1)} \right)_a; 0, \sigma_p^2 \right) \right. \right. \\ & \quad \left. \left. + \sum_{b=1}^d G_{i,b}^\top \log \mathcal{N} \left(\Theta_{a,b}^{(i,1)}; 0, \sigma_p^2 \right) \right) \right. \\ & \quad \left. + \sum_{l=2}^L \sum_{a=1}^{d_l} \left(\log \mathcal{N} \left(\left(\theta_b^{(i,l)} \right)_a; 0, \sigma_p^2 \right) \right. \right. \\ & \quad \left. \left. + \sum_{b=1}^{d_{l-1}} \log \mathcal{N} \left(\Theta_{a,b}^{(i,l)}; 0, \sigma_p^2 \right) \right) \right), \end{aligned} \quad (12)$$

where σ_p is the standard deviation of the Gaussian parameters. In the nonlinear Gaussian setting, the value of $f_i(\mathbf{X}_{pa(i)})$ is assumed to be the mean of the distribution of each variable X_i . As a result, the log likelihood of this model is as follows

$$\begin{aligned} & \log p(\mathcal{D} | \mathbf{G}, \Theta) \\ &= \sum_{i=1}^d \log \mathcal{N} \left(X_i; \text{FFN} \left(\mathbf{G}_i^\top \circ \mathbf{X}; \Theta^{(i)} \right), \sigma_{obs}^2 \right), \end{aligned} \quad (13)$$

where “ \circ ” denotes the element-wise multiplication.

D. Particle Variational Inference of Intractable Posterior

The joint posterior distribution $p(\mathbf{Z}, \Theta | \mathcal{D}, \mathbf{P})$ is intractable. Stein variational gradient descent (SVGD) [24], [25] is a suitable method to approximate this joint posterior density due to its gradient-based approach. The SVGD algorithm iteratively transports a set of particles to match the target distribution similar to the gradient descent algorithm in optimization.

From the proposed generative model, we need to infer the log joint posterior density of \mathbf{Z} and Θ using the corresponding gradient to variable \mathbf{Z} given by

$$\begin{aligned} & \nabla_{\mathbf{Z}} \log p(\mathbf{Z}, \Theta | \mathcal{D}, \mathbf{P}) \\ &= \nabla_{\mathbf{Z}} \log p(\mathbf{Z}) + \frac{\nabla_{\mathbf{Z}} \mathbb{E}_{p(\mathbf{G}|\mathbf{Z}, \mathbf{P})} [p(\Theta, \mathcal{D} | \mathbf{G})]}{\mathbb{E}_{p(\mathbf{G}|\mathbf{Z}, \mathbf{P})} [p(\Theta, \mathcal{D} | \mathbf{G})]}. \end{aligned} \quad (14)$$

The log latent prior distribution $\log p(\mathbf{Z})$ is chosen as

$$\begin{aligned} \log p(\mathbf{Z}) &:= \sum_{i,j} \log \mathcal{N}(U_{ij}; 0, \sigma_z^2) + \sum_{i,j} \log \mathcal{N}(V_{ij}; 0, \sigma_z^2) \\ & \quad + \mathbb{E}_{p(\mathbf{G}|\mathbf{Z}, \mathbf{P})} [\log p(\mathbf{G} | \mathbf{Z}, \mathbf{P})] - C, \end{aligned} \quad (15)$$

where C is the log partitioning constant. Similarly, the gradient corresponding to variable Θ is given by

$$\nabla_{\Theta} \log p(\mathbf{Z}, \Theta | \mathcal{D}, \mathbf{P}) = \frac{\nabla_{\Theta} \mathbb{E}_{p(\mathbf{G}|\mathbf{Z}, \mathbf{P})} [p(\Theta, \mathcal{D} | \mathbf{G})]}{\mathbb{E}_{p(\mathbf{G}|\mathbf{Z}, \mathbf{P})} [p(\Theta, \mathcal{D} | \mathbf{G})]}. \quad (16)$$

The numerator of the second term in Equation (14) can be approximated using the Gumbel-softmax trick [19], [27] as follows

$$\begin{aligned} & \nabla_{\Theta} \mathbb{E}_{p(\mathbf{G}|\mathbf{Z}, \mathbf{P})} [p(\Theta, \mathcal{D} | \mathbf{G})] \\ & \approx \mathbb{E}_{p(\mathbf{L})} \left[\left. \nabla_{\mathbf{G}} p(\Theta, \mathcal{D} | \mathbf{G}) \right|_{\mathbf{G}=\tilde{\mathbf{G}}_\tau(\mathbf{L}, \mathbf{Z})} \cdot \nabla_{\mathbf{Z}} \tilde{\mathbf{G}}_\tau(\mathbf{L}, \mathbf{Z}) \right], \end{aligned} \quad (17)$$

where $\mathbf{L} \sim \text{Logistic}(0, 1)^{(d-1) \times (d-1)}$ and the matrix $\tilde{\mathbf{G}}_\tau(\mathbf{L}, \mathbf{Z}) = \mathbf{P} \tilde{\mathbf{S}}_\tau(\mathbf{L}, \mathbf{Z}) \mathbf{P}^\top$. The element-wise definition of $\tilde{\mathbf{S}}_\tau$ is

$$\tilde{\mathbf{S}}_\tau(\mathbf{L}, \mathbf{Z})_{i,j} := \begin{cases} \sigma_\tau (L_{i,j-1} + \alpha \mathbf{u}_i^\top \mathbf{v}_{j-1}) & \text{if } j > i, \\ 0 & \text{otherwise.} \end{cases} \quad (18)$$

In our experiments, we choose $\tau = 1$ in accordance with [25].

The kernel for SVGD proposed in [25] is

$$\begin{aligned} & k((\mathbf{Z}, \Theta), (\mathbf{Z}', \Theta')) \\ & := \exp \left(-\frac{1}{\gamma_z} \|\mathbf{Z} - \mathbf{Z}'\|_2^2 \right) + \exp \left(-\frac{1}{\gamma_\theta} \|\Theta - \Theta'\|_2^2 \right). \end{aligned} \quad (19)$$

From this kernel, an incremental update for the m th particle of \mathbf{Z} at the t th step is computed by

$$\begin{aligned} & \phi_t^{\mathbf{Z}}(\mathbf{Z}_t^{(m)}, \Theta_t^{(m)}) \\ &= \frac{1}{M} \sum_{r=1}^M \left[k \left((\mathbf{Z}_t^{(r)}, \Theta_t^{(r)}), (\mathbf{Z}_t^{(m)}, \Theta_t^{(m)}) \right) \right. \\ & \quad \cdot \nabla_{\mathbf{Z}_t^{(r)}} \log p(\mathbf{Z}_t^{(r)}, \Theta_t^{(r)} | \mathcal{D}, \mathbf{P}) \\ & \quad \left. + \nabla_{\mathbf{Z}_t^{(r)}} k \left((\mathbf{Z}_t^{(r)}, \Theta_t^{(r)}), (\mathbf{Z}_t^{(m)}, \Theta_t^{(m)}) \right) \right]. \end{aligned} \quad (20)$$

A similar update for Θ is proposed by replacing $\nabla_{\mathbf{Z}_t^{(r)}}$ by $\nabla_{\Theta_t^{(r)}}$ as

$$\begin{aligned} & \phi_t^{\Theta}(\mathbf{Z}_t^{(m)}, \Theta_t^{(m)}) \\ &= \frac{1}{M} \sum_{r=1}^M \left[k \left((\mathbf{Z}_t^{(r)}, \Theta_t^{(r)}), (\mathbf{Z}_t^{(m)}, \Theta_t^{(m)}) \right) \right. \\ & \quad \cdot \nabla_{\Theta_t^{(r)}} \log p(\mathbf{Z}_t^{(r)}, \Theta_t^{(r)} | \mathcal{D}, \mathbf{P}) \\ & \quad \left. + \nabla_{\Theta_t^{(r)}} k \left((\mathbf{Z}_t^{(r)}, \Theta_t^{(r)}), (\mathbf{Z}_t^{(m)}, \Theta_t^{(m)}) \right) \right]. \end{aligned} \quad (21)$$

The SVGD algorithm for inferring $p(\mathbf{G}, \Theta | \mathcal{D}, \mathbf{P})$ is represented in Algorithm 1.

Algorithm 1 SVGD algorithm for inference of $p(\mathbf{G}, \Theta \mid \mathcal{D}, \mathbf{P})$

Input: Initial set of latent and parameter particles $\left\{ \left(\mathbf{Z}_0^{(m)}, \Theta_0^{(m)} \right) \right\}_{m=1}^M$, kernel k , schedules for η_t, α_t , observational data \mathcal{D} , and permutation matrix \mathbf{P}

Output: Set of adjacency matrices and parameter particles $\left\{ \left(\mathbf{G}^{(m)}, \Theta^{(m)} \right) \right\}_{m=1}^M$

- 1) Incorporate prior belief of $p(\mathbf{G} \mid \mathbf{Z}, \mathbf{P})$ into $p(\mathbf{Z})$
 - 2) **for** iteration $t = 0$ to $T - 1$ **do**
 - 3) Estimate score $\nabla_{\mathbf{Z}} \log p(\mathbf{Z}, \Theta \mid \mathcal{D}, \mathbf{P})$ given in Equation (14) for every $\mathbf{Z}_t^{(m)}$
 - 4) Estimate score $\nabla_{\Theta} \log p(\mathbf{Z}, \Theta \mid \mathcal{D}, \mathbf{P})$ given in Equation (16) for every $\Theta_t^{(m)}$
 - 5) **for** particle $m = 1$ to M **do**
 - 6) $\mathbf{Z}_{t+1}^{(m)} \leftarrow \mathbf{Z}_t^{(m)} + \eta_t \phi_t^{\mathbf{Z}} \left(\mathbf{Z}_t^{(m)}, \Theta_t^{(m)} \right), \left(\phi_t^{\mathbf{Z}} \left(\mathbf{Z}_t^{(m)}, \Theta_t^{(m)} \right) \right)$ from Equation (20)
 - 7) $\Theta_{t+1}^{(m)} \leftarrow \Theta_t^{(m)} + \eta_t \phi_t^{\Theta} \left(\mathbf{Z}_t^{(m)}, \Theta_t^{(m)} \right), \left(\phi_t^{\Theta} \left(\mathbf{Z}_t^{(m)}, \Theta_t^{(m)} \right) \right)$ from Equation (21)
 - 8) **return** $\left\{ \left(\mathbf{G}_{\infty}^{(m)} = \mathbf{P} \mathbf{S}_{\infty} \left(\mathbf{Z}_T^{(m)} \right) \mathbf{P}^{\top}, \Theta_T^{(m)} \right) \right\}_{m=1}^M$
-

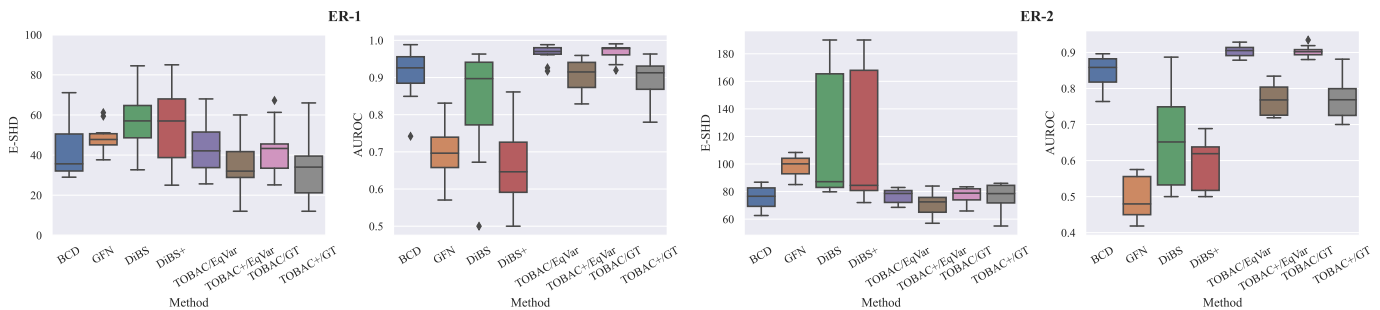


Fig. 2. Performance on synthetic data generated from linear Gaussian models with $d = 20$ variables, $n = 100$ observations, and 1000 sampling steps. Lower E-SHD and higher AUROC are preferable. Our TOBAC models with the orderings from EqVar [5] and the ground-truth orderings are compared with BCD Nets (denoted as BCD) [8], DAG-GFlowNet (denoted as GFN) [9], and DiBS [25]. The DiBS+ and TOBAC+ models are the results with weighted particle mixture. All the methods except for DiBS are designed to ensure acyclicity, so the cyclicity score is not necessary. The different designs of BCD Nets and DAG-GFlowNet make the comparison by the negative log likelihood evaluation with the joint posterior distribution implausible. Our TOBAC models accomplish the lowest E-SHD scores and the almost highest AUROC scores in both ER-1 (sparse graph) and ER-2 (denser graph) settings.

IV. EXPERIMENTS

A. Experimental Settings

We compare our TOBAC approach with related Bayesian score-based methods including BCD Nets [8], DAG-GFlowNet (GFN) [9], and DiBS [25] on synthetic and the flow cytometry data [36]. Beside DiBS, which can learn the joint distribution $p(\mathbf{G}, \Theta \mid \mathcal{D})$ and infer nonlinear Gaussian networks, BCD Nets and DAG-GFlowNet are designed to work with linear Gaussian models. BCD Nets learns the parameters using the weighted adjacency matrix and DAG-GFlowNet uses the BGe score [15].

Regarding the selection of topological ordering for conditioning, we choose the topological ordering from EqVar [5] and the ground-truth (GT) ordering as the condition for our approach. We also analyze the effect of the ordering on the performance by replacing the ordering with the one from NPVar [14] and SCORE [35]. The DiBS+ and TOBAC+ denotations in our experiments are the results with weighted particle mixture in [25] that use $p(\mathbf{G}, \Theta, \mathcal{D})$ as the weight for each particle. This weight is employed as the unnormalized probability for each inferred particle when computing the expectation of the evaluation metrics.

a) *Synthetic data & graph prior:* We generate the data using the Erdős–Rényi (ER) structure [12] with the degree of 1 and 2. In all settings in Section IV-B, each inference is performed on $n = 100$ observations. For the ablation study in Section IV-D, synthetic data with $d \in \{10, 20, 50\}$ variables and $n \in \{100, 500\}$ observations is utilized for the analysis of the effect of dimensionality and sample size on the performance. For the graph prior, BCD Nets uses the Horseshoe prior for their strictly lower triangular matrix \mathbf{L} , and GFN uses the prior from [11]. DiBS and our approach use the prior of the Erdős–Rényi graphs, which is in the form of $p(\mathbf{G}) \propto q^{\|\mathbf{G}\|_1} (1 - q)^{\binom{d}{2} - \|\mathbf{G}\|_1}$ where q is the probability for an independent edge being added to the DAG.

b) *Evaluation metrics:* Following the evaluation metrics used by previous work [9], [8], [25], we evaluate the performance using the *expected structural Hamming distance* (E-SHD) and *area under the receiver operating characteristic curve* (AUROC). We follow [25] where the E-SHD score is the expectation of the *structural Hamming distance* (SHD) between each \mathbf{G} and the ground-truth \mathbf{G}^* over the posterior distribution $p(\mathbf{G} \mid \mathcal{D})$ to compute the expected number of edges that has been incorrectly predicted. The formulation of

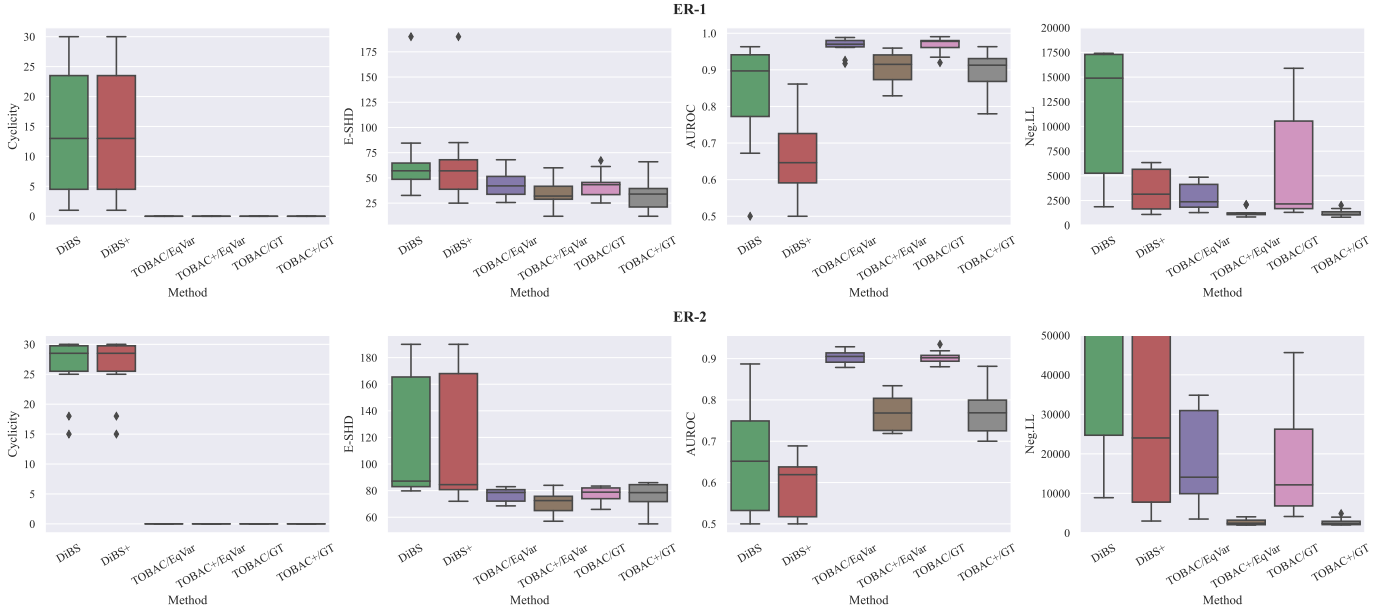


Fig. 3. Performance on synthetic data generated from nonlinear Gaussian models with $d = 20$ variables, $n = 100$ observations, and 1000 sampling steps. Lower Cyclcity, E-SHD, and Neg.LL, and higher AUROC are preferable. Our TOBAC models with the orderings from EqVar [5] and the ground-truth orderings are compared with DiBS [25]. The DiBS+ and TOBAC+ models are the results with weighted particle mixture. Note that BCD Nets [8] and DAG-GFlowNet [9] are only designed for linear Gaussian models, so these methods are not included in this experiment. In comparison with DiBS, our TOBAC models can guarantee the acyclicity of the learned graphs. Our models also perform better in all evaluation metrics and show more stable results with fewer variances, especially in denser ER-2 graphs.

this evaluation score is

$$\text{E-SHD}(p, \mathbf{G}^*) := \sum_{\mathbf{G}} p(\mathbf{G} | \mathcal{D}) \text{SHD}(\mathbf{G}, \mathbf{G}^*). \quad (22)$$

The AUROC score is computed for each edge probability $p(G_{i,j} = 1 | \mathcal{D})$ in comparison with the corresponding ground-truth edge in \mathbf{G}^* [18]. In addition, we also evaluate the nonlinear Gaussian Bayesian networks from DiBS and ours by the *cyclcity* score and the average *negative log likelihood* [25]. The cyclcity score is proposed by [44] and is used in DiBS as the constraint for acyclicity. The score measuring the cyclcity or non-DAG-ness of a graph \mathbf{G} is defined as

$$h(\mathbf{G}) := \text{tr} \left[\left(\mathbf{I} + \frac{1}{d} \mathbf{G} \right)^d \right] - d, \quad (23)$$

where $h(\mathbf{G}) = 0$ if and only if \mathbf{G} has no cycle and the higher its value, the more cyclic \mathbf{G} becomes. In the average negative log likelihood evaluation, a test dataset \mathcal{D}^{test} containing 100 held-out observations are also generated to compute the score as follows

$$\begin{aligned} \text{Neg.LL}(p, \mathcal{D}^{test}) \\ := - \sum_{\mathbf{G}, \Theta} p(\mathbf{G}, \Theta | \mathcal{D}) \log p(\mathcal{D}^{test} | \mathbf{G}, \Theta). \end{aligned} \quad (24)$$

This score is designed to evaluate the model's ability to predict future observations. Note that BCD Nets formulates the parameters with the weighted adjacency matrix, and DAG-GFlowNet only estimates the marginal posterior distribution $p(\mathbf{G} | \mathcal{D})$ and uses BGe score [15] for the parameters. Hence, we cannot

compute the joint posterior distribution $p(\mathbf{G}, \Theta | \mathcal{D})$ for the negative log likelihood evaluation. The reported results in the following sections are obtained from ten randomly generated datasets for each method and configuration.

B. Performance on Synthetic Data

a) *Linear Gaussian models*: Figure 2 illustrates the performance of the methods with linear Gaussian models. We find that our TOBAC and TOBAC+ outperform other approaches. TOBAC models accomplish the lowest E-SHD scores and the almost highest AUROC scores in both ER-1 (sparse graph) and ER-2 (denser graph) settings. In comparison with DiBS, the results demonstrate that by introducing the prior knowledge, which is the EqVar and ground-truth orderings, to the inference process can increase the performance significantly. As the graph becomes denser, as in the ER-2 settings, DiBS models have high variances in the results, whereas our models are as stable as other approaches. Considering DAG-GFlowNet, which uses GFlowNets [2] to infer the posterior distribution, our models achieve lower E-SHD score and substantially higher AUROC score in the denser graph setting.

b) *Nonlinear Gaussian models*: The performance results of nonlinear Gaussian models are depicted in Figure 3. The cyclcity scores clearly show that the acyclicity constraint of DiBS is not as effective compared to our approach. In addition to the certainty of acyclicity, from all the E-SHD, AUROC, and negative log likelihood scores, we can see that our approaches can infer better graphs than DiBS. This improvement in performance emphasizes the benefit of the orderings while guaranteeing the acyclicity at every number of sampling steps.

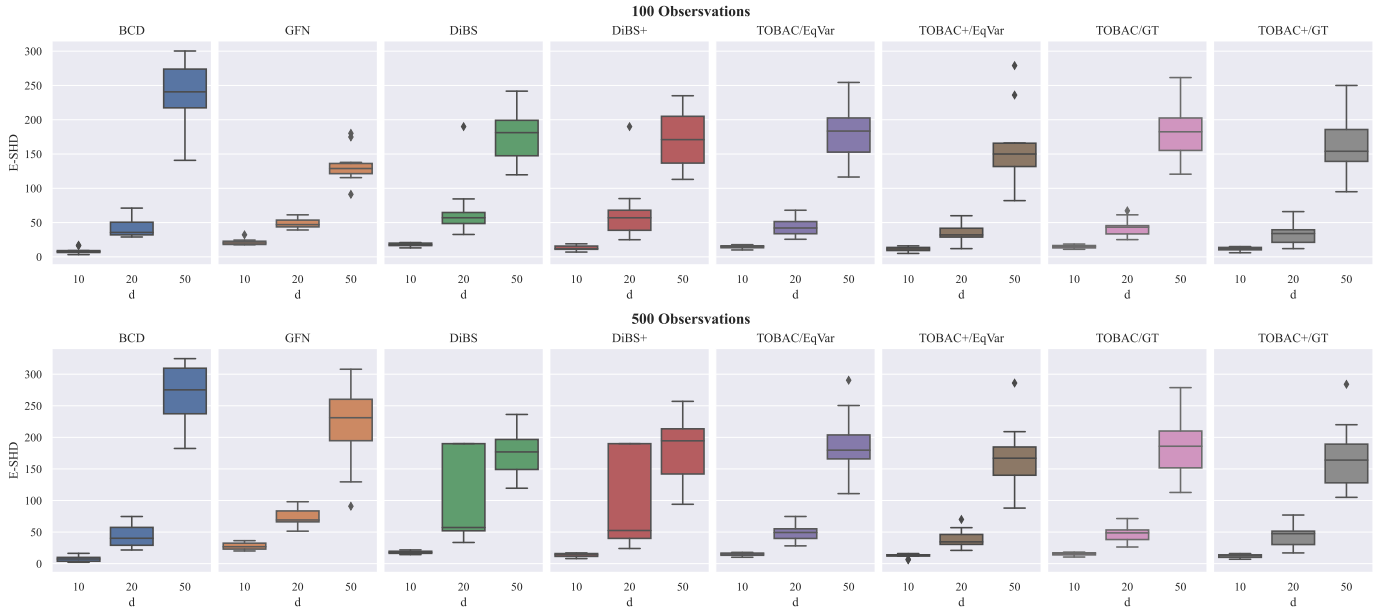


Fig. 4. Expected structural Hamming distance on synthetic data with different sample sizes and dimensionalities. Lower E-SHD is preferable. Our TOBAC models with the orderings from EqVar [5] and the ground-truth orderings are compared with BCD Nets (denoted as BCD) [8], DAG-GFlowNet (denoted as GFN) [9], and DiBS [25]. The DiBS+ and TOBAC+ models are the results with weighted particle mixture. Our models can learn more accurate graphs with more stable results when the data’s dimension increases. Most approaches are not affected by the number of observations, except for DAG-GFlowNet (GFN) [9], which cannot learn as effectively due to the incapability to handle higher peakness of the posterior distribution.

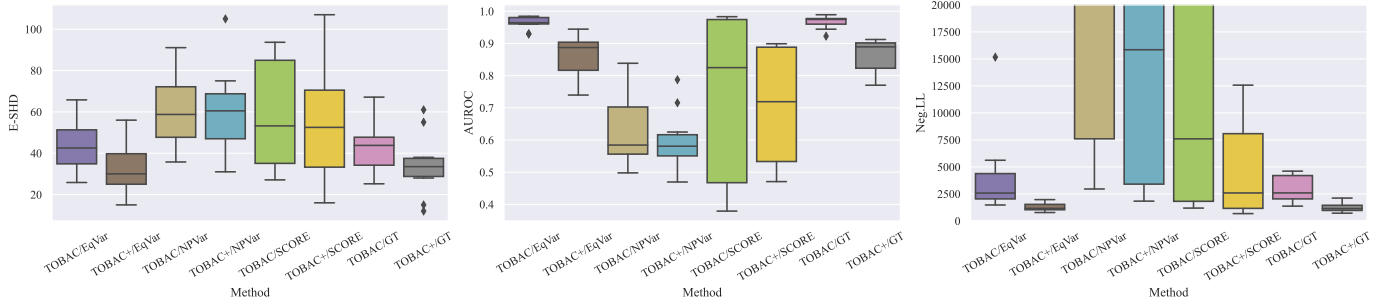


Fig. 5. Performance with topological orderings from different methods in the linear setting with $d = 20$ variables, $n = 100$ observations, and 1000 sampling steps. Lower E-SHD and Neg.LL, and higher AUROC are preferable. The TOBAC models with the orderings from EqVar [5], NPVar [14], and SCORE [35] are compared with the models with ground-truth orderings. The TOBAC+ models are the results with weighted particle mixture. The experiments are configured with equal variance, so our models with orderings from EqVar [5] can accomplish similar results to the ones with the ground-truth orderings. The assumption of nonlinearity in the setting of SCORE makes the models with its orderings less stable.

With the orderings given, optimizing the graph parameters become significantly easier. As a result, the log likelihood of the observational data is improved. Furthermore, the plots in the ER-2 indicate that TOBAC is more stable than DiBS when inferring denser graphs.

C. Performance on Real Data

The flow cytometry dataset includes $n = 853$ observational continuous data points and $d = 11$ phosphoproteins. The graphs are inferred with linear Gaussian models and Erdős–Rényi graph priors at 1000 sampling steps. As we can observe in Table I, our TOBAC and TOBAC+ approaches with the orderings from EqVar has achieved the lowest E-SHD values at 15.6 ± 0.42 and 14.8 ± 1.13 respectively. Additionally, the AUROC score of TOBAC is the second highest one at

TABLE I
PERFORMANCE ON THE FLOW CYTOMETRY DATASET [36].
REPORTED RESULTS ARE THE MEAN \pm STD OF THE METRICS.
THE BEST RESULTS ARE PRESENTED IN **BOLD** STYLE.
OUR METHODS ACHIEVE THE BEST E-SHD SCORE AND THE SECOND HIGHEST AUROC SCORE IN COMPARISON WITH RELATED APPROACHES.

	E-SHD↓	AUROC↑
BCD [8]	17.1 ± 0.13	0.534 ± 0.0640
GFN [9]	21.2 ± 1.50	0.496 ± 0.0609
DiBS [25]	15.9 ± 0.41	0.625 ± 0.0367
DiBS+ [25]	15.4 ± 1.35	0.553 ± 0.0494
TOBAC/EqVar	15.6 ± 0.42	0.599 ± 0.0395
TOBAC+/EqVar	14.8 ± 1.13	0.560 ± 0.0309

0.599 ± 0.0395 , which is lower than DiBS’s at 0.625 ± 0.0367 . Moreover, TOBAC+’s AUROC score is slightly higher than DiBS+’s score at 0.560 ± 0.0309 compared to 0.553 ± 0.0494 .

a) *Sample sizes & dimensionalities*: We study the effect of different sample sizes and data dimensionalities on TOBAC and related approaches. As we can perceive in Figure 4, the number of observations does not have much effect on the performance in most cases. In the case of GFN, as also described by Deleu et al. [9], when the number of observations increases, this model can not perform as well as with a smaller sample size due to the higher peakness of the posterior distribution. These results show that Bayesian approaches can sufficiently handle the uncertainty caused by a smaller amount of data. In contrast, as the number of dimensions in the data rises, the effect on the inference performance diverges among the approaches. Graphs with 50 nodes inferred by TOBAC are more accurate in comparison with other approaches.

b) *Topological orderings from other approaches*: We summarize the results of the graphs inferred by TOBAC with the ground-truth ordering and the orderings learned by several approaches consisting of EqVar [5], NPVar [14], and SCORE [35] in Figure 5. In this setting, the variances of the variables are equal, which are matched to EqVar settings. As a consequence, the results suggest that TOBAC with EqVar can have the performance scores that are close to TOBAC with the ground-truth ordering on synthetic data. Although being the state-of-the-art approach in learning the ordering, the results when employing SCORE are more unstable in comparison with other simpler ones. This unstable may be due to the nonlinear assumption of the structural equation model in SCORE, which does not fit well with this linear Gaussian setting.

c) *Uniform & weighted particle mixture*: From the observed results, the weighted particle mixture can reduce the E-SHD and Neg.LL scores. However, it will also cause a reduction in the AUROC scores. The lower performance of the uniform mixture can be due to the crude approximation of the particles' posterior probability mass function, which is replaced by a more meaningful approach in the weighted mixture [25].

V. CONCLUSION

In this work, we have presented TOBAC—an approach to strictly constraining the acyclicity of the inferred graphs and integrating the knowledge from the topological orderings into the inference process. Our work uses a continuous representation of the canonical adjacency matrix and approximate the posterior using particle variational inference. Our proposed framework makes the inference process less complicated and enhances the accuracy of inferred graphs and parameters. Accordingly, our work can outperform most related Bayesian score-based approaches on both synthetic and real observational data. In future work, we will explore methods to learn the posterior distribution of the topological orderings with observational data, which will allow our approach to infer more diverse posterior distributions while still ensuring the acyclicity of generated graphs.

- [1] A.-L. Barabási and R. Albert, "Emergence of scaling in random networks," *Science*, vol. 286, no. 5439, pp. 509–512, 1999.
- [2] Y. Bengio, S. Lahlou, T. Deleu, E. J. Hu, M. Tiwari, and E. Bengio, "GFlowNet foundations," *arXiv preprint arXiv:2111.09266*, 2022.
- [3] J. Bradbury, R. Frostig, P. Hawkins, M. J. Johnson, C. Leary, D. Maclaurin, G. Necula, A. Paszke, J. VanderPlas, S. Wanderman-Milne, and Q. Zhang, "JAX: composable transformations of Python+NumPy programs," 2018.
- [4] P. Bühlmann, J. Peters, and J. Ernest, "CAM: Causal additive models, high-dimensional order search and penalized regression," *The Annals of Statistics*, vol. 42, no. 6, pp. 2526–2556, 2014.
- [5] W. Chen, M. Drton, and Y. S. Wang, "On causal discovery with an equal-variance assumption," *Biometrika*, vol. 106, no. 4, pp. 973–980, 2019.
- [6] D. M. Chickering, "Optimal structure identification with greedy search," *Journal of Machine Learning Research*, vol. 3, pp. 507–554, 2002.
- [7] M. Chickering, D. Heckerman, and C. Meek, "Large-sample learning of Bayesian networks is NP-hard," *Journal of Machine Learning Research*, vol. 5, pp. 1287–1330, 2004.
- [8] C. Cundy, A. Grover, and S. Ermon, "BCD Nets: Scalable variational approaches for Bayesian causal discovery," in *Advances in Neural Information Processing Systems*, vol. 34, 2021, pp. 7095–7110.
- [9] T. Deleu, A. Góis, C. Emezue, M. Rankawat, S. Lacoste-Julien, S. Bauer, and Y. Bengio, "Bayesian structure learning with generative flow networks," in *Proceedings of Conference on Uncertainty in Artificial Intelligence*, ser. Proceedings of Machine Learning Research, vol. 180, 2022, pp. 518–528.
- [10] T. Deleu, M. Nishikawa-Toomey, J. Subramanian, N. Malkin, L. Charlin, and Y. Bengio, "Joint bayesian inference of graphical structure and parameters with a single generative flow network," *arXiv preprint arXiv:2305.19366*, 2023.
- [11] R. Eggeling, J. Viinikka, A. Vuoksenmaa, and M. Koivisto, "On structure priors for learning Bayesian networks," in *Proceedings of the International Conference on Artificial Intelligence and Statistics*, ser. Proceedings of Machine Learning Research, vol. 89, 2019, pp. 1687–1695.
- [12] P. Erdős and A. Rényi, "On the evolution of random graphs," *Publications of the Mathematical Institute of the Hungarian Academy of Sciences*, vol. 5, 1960.
- [13] N. Friedman, M. Goldszmidt, and A. Wyner, "Data analysis with Bayesian networks: A bootstrap approach," in *Proceedings of the Conference on Uncertainty in Artificial Intelligence*, 1999, pp. 196–205.
- [14] M. Gao, Y. Ding, and B. Aragam, "A polynomial-time algorithm for learning nonparametric causal graphs," in *Advances in Neural Information Processing Systems*, vol. 33, 2020, pp. 11 599–11 611.
- [15] D. Geiger and D. Heckerman, "Learning Gaussian networks," in *Proceedings of the Conference on Uncertainty in Artificial Intelligence*, 1994, pp. 235–243.
- [16] A. A. Hagberg, D. A. Schult, and P. J. Swart, "Exploring network structure, dynamics, and function using NetworkX," in *Proceedings of the Python in Science Conference*, 2008, pp. 11–15.
- [17] C. R. Harris, K. J. Millman, S. J. van der Walt, R. Gommers, P. Virtanen, D. Cournapeau, E. Wieser, J. Taylor, S. Berg, N. J. Smith, R. Kern, M. Picus, S. Hoyer, M. H. van Kerkwijk, M. Brett, A. Haldane, J. F. del Río, M. Wiebe, P. Peterson, P. Gérard-Marchant, K. Sheppard, T. Reddy, W. Weckesser, H. Abbasi, C. Gohlke, and T. E. Oliphant, "Array programming with NumPy," *Nature*, vol. 585, no. 7825, pp. 357–362, 2020.
- [18] D. Husmeier, "Sensitivity and specificity of inferring genetic regulatory interactions from microarray experiments with dynamic Bayesian networks," *Bioinformatics*, vol. 19, no. 17, pp. 2271–2282, 2003.
- [19] E. Jang, S. Gu, and B. Poole, "Categorical reparameterization with Gumbel-softmax," in *Proceedings of the International Conference on Learning Representations*, 2017.
- [20] M. Koivisto, "Advances in exact Bayesian structure discovery in Bayesian networks," in *Proceedings of the Conference on Uncertainty in Artificial Intelligence*, 2006, pp. 241–248.
- [21] D. Koller and N. Friedman, *Probabilistic graphical models: principles and techniques*. MIT press, 2009.
- [22] S. Lachapelle, P. Brouillard, T. Deleu, and S. Lacoste-Julien, "Gradient-based neural DAG learning," *arXiv preprint arXiv:1906.02226*, 2019.

- [23] H.-C. Lee, M. Danieletto, R. Miotto, S. T. Cherng, and J. T. Dudley, “Scaling structural learning with NO-BEARS to infer causal transcriptome networks,” in *Pacific Symposium on Biocomputing 2020*, 2019, pp. 391–402.
- [24] Q. Liu and D. Wang, “Stein variational gradient descent: A general purpose Bayesian inference algorithm,” in *Advances in Neural Information Processing Systems*, vol. 29, 2016.
- [25] L. Lorch, J. Rothfuss, B. Schölkopf, and A. Krause, “DiBS: Differentiable Bayesian structure learning,” in *Advances in Neural Information Processing Systems*, vol. 34, 2021, pp. 24 111–24 123.
- [26] L. Lorch, S. Sussex, J. Rothfuss, A. Krause, and B. Schölkopf, “Amortized inference for causal structure learning,” *arXiv preprint arXiv:2205.12934*, 2022.
- [27] C. J. Maddison, A. Mnih, and Y. W. Teh, “The concrete distribution: A continuous relaxation of discrete random variables,” in *Proceedings of the International Conference on Learning Representations*, 2017.
- [28] D. Madigan, J. York, and D. Allard, “Bayesian graphical models for discrete data,” *International Statistical Review / Revue Internationale de Statistique*, vol. 63, no. 2, pp. 215–232, 1995.
- [29] U. Manber, *Introduction to algorithms: A creative approach*. Addison-Wesley Longman Publishing Co., Inc., 1989.
- [30] C. Molnar, G. Casalicchio, and B. Bischl, “Interpretable machine learning – a brief history, state-of-the-art and challenges,” in *Proceedings of the Joint European Conference on Machine Learning and Knowledge Discovery in Databases Workshops*, 2020, pp. 417–431.
- [31] F. Montagna, N. Noceti, L. Rosasco, K. Zhang, and F. Locatello, “Scalable causal discovery with score matching,” in *Proceedings of the Conference on Neural Information Processing Systems Workshop on Score-Based Methods*, 2022.
- [32] M. Nishikawa-Toomey, T. Deleu, J. Subramanian, Y. Bengio, and L. Charlin, “Bayesian learning of causal structure and mechanisms with GFlowNets and variational Bayes,” *arXiv preprint arXiv:2211.02763*, 2022.
- [33] A. Paszke, S. Gross, F. Massa, A. Lerer, J. Bradbury, G. Chanan, T. Killeen, Z. Lin, N. Gimelshein, L. Antiga *et al.*, “PyTorch: An imperative style, high-performance deep learning library,” in *Advances in Neural Information Processing Systems*, vol. 32, 2019.
- [34] G. Raskutti and C. Uhler, “Learning directed acyclic graph models based on sparsest permutations,” *Stat*, vol. 7, no. 1, p. e183, 2018.
- [35] P. Rolland, V. Cevher, M. Kleindessner, C. Russell, D. Janzing, B. Schölkopf, and F. Locatello, “Score matching enables causal discovery of nonlinear additive noise models,” in *Proceedings of the International Conference on Machine Learning*, ser. Proceedings of Machine Learning Research, vol. 162, 2022, pp. 18 741–18 753.
- [36] K. Sachs, O. Perez, D. Pe’er, D. A. Lauffenburger, and G. P. Nolan, “Causal protein-signaling networks derived from multiparameter single-cell data,” *Science*, vol. 308, no. 5721, pp. 523–529, 2005.
- [37] P. Sanchez, X. Liu, A. Q. O’Neil, and S. A. Tsafaris, “Diffusion models for causal discovery via topological ordering,” in *Proceedings of the International Conference on Learning Representations*, 2023.
- [38] D. Servén and C. Brummitt, “pyGAM: Generalized additive models in Python,” Mar. 2018.
- [39] L. Solus, Y. Wang, and C. Uhler, “Consistency guarantees for greedy permutation-based causal inference algorithms,” *Biometrika*, vol. 108, no. 4, pp. 795–814, 2021.
- [40] P. Spirtes, C. Glymour, and R. Scheines, *Causation, Prediction, and Search*, ser. Adaptive Computation and Machine Learning Series. The MIT Press, 2000.
- [41] C. Squires and C. Uhler, “Causal structure learning: A combinatorial perspective,” *Foundations of Computational Mathematics*, pp. 1–35, 2022.
- [42] C. Squires, Y. Wang, and C. Uhler, “Permutation-based causal structure learning with unknown intervention targets,” in *Proceedings of the Conference on Uncertainty in Artificial Intelligence*, ser. Proceedings of Machine Learning Research, vol. 124, 2020, pp. 1039–1048.
- [43] Y. Wang, L. Solus, K. Yang, and C. Uhler, “Permutation-based causal inference algorithms with interventions,” *Advances in Neural Information Processing Systems*, vol. 30, 2017.
- [44] Y. Yu, J. Chen, T. Gao, and M. Yu, “DAG-GNN: DAG structure learning with graph neural networks,” in *Proceedings of the International Conference on Machine Learning*, ser. Proceedings of Machine Learning Research, vol. 97, 2019, pp. 7154–7163.
- [45] R. Zhao, X. He, and J. Wang, “Learning linear non-Gaussian directed acyclic graph with diverging number of nodes,” *Journal of Machine Learning Research*, vol. 23, no. 269, pp. 1–34, 2022.
- [46] X. Zheng, B. Aragam, P. K. Ravikumar, and E. P. Xing, “DAGs with NO-TEARS: Continuous optimization for structure learning,” in *Advances in Neural Information Processing Systems*, vol. 31, 2018.
- [47] X. Zheng, C. Dan, B. Aragam, P. Ravikumar, and E. Xing, “Learning sparse nonparametric DAGs,” in *Proceedings of the International Conference on Artificial Intelligence and Statistics*, vol. 108, 2020, pp. 3414–3425.

APPENDIX A PROOF OF EQUATION (8)

First, we will recall the generative model in Equation (7), which states that

$$p(\mathbf{Z}, \mathbf{S}, \mathbf{G}, \Theta, \mathcal{D} | \mathbf{P}) = p(\mathbf{Z}) p(\mathbf{S} | \mathbf{Z}) p(\mathbf{G} | \mathbf{S}, \mathbf{P}) p(\Theta | \mathbf{G}) p(\mathcal{D} | \mathbf{G}, \Theta)$$

In addition, from Bayes’ theorem, we have

$$p(\mathbf{Z}) = \frac{p(\mathcal{D}) p(\mathbf{Z}, \Theta | \mathcal{D}, \mathbf{P})}{p(\Theta, \mathcal{D} | \mathbf{Z}, \mathbf{P})} \Rightarrow \frac{p(\mathbf{Z})}{p(\mathcal{D})} = \frac{p(\mathbf{Z}, \Theta | \mathcal{D}, \mathbf{P})}{p(\Theta, \mathcal{D} | \mathbf{Z}, \mathbf{P})}.$$

Proof: The proof of the computation for expectation of $f(\mathbf{G}, \Theta)$ with $(\mathbf{G}, \Theta) \sim p(\mathbf{G}, \Theta | \mathcal{D}, \mathbf{P})$ in Equation (8) is as follows

$$\begin{aligned} & \mathbb{E}_{p(\mathbf{G}, \Theta | \mathcal{D}, \mathbf{P})} [f(\mathbf{G}, \Theta)] \\ &= \sum_{\mathbf{G}} \int_{\Theta} p(\mathbf{G}, \Theta | \mathcal{D}, \mathbf{P}) f(\mathbf{G}, \Theta) d\Theta \\ &= \sum_{\mathbf{G}} \int_{\Theta} \frac{p(\mathbf{G}, \Theta, \mathcal{D} | \mathbf{P}) f(\mathbf{G}, \Theta)}{p(\mathcal{D})} d\Theta \\ &= \sum_{\mathbf{G}} \int_{\Theta} \sum_{\mathbf{S}} \int_{\mathbf{Z}} \frac{p(\mathbf{Z}, \mathbf{S}, \mathbf{G}, \Theta, \mathcal{D} | \mathbf{P}) f(\mathbf{G}, \Theta)}{p(\mathcal{D})} d\mathbf{Z} d\Theta \\ &= \sum_{\mathbf{G}} \int_{\Theta} \sum_{\mathbf{S}} \int_{\mathbf{Z}} \frac{1}{p(\mathcal{D})} p(\mathbf{Z}) p(\mathbf{S} | \mathbf{Z}) p(\mathbf{G} | \mathbf{S}, \mathbf{P}) \cdot \\ & \quad p(\Theta | \mathbf{G}) p(\mathcal{D} | \mathbf{G}, \Theta) f(\mathbf{G}, \Theta) d\mathbf{Z} d\Theta \\ &= \int_{\Theta} \int_{\mathbf{Z}} \frac{p(\mathbf{Z})}{p(\mathcal{D})} \sum_{\mathbf{G}} \sum_{\mathbf{S}} p(\mathbf{S} | \mathbf{Z}) p(\mathbf{G} | \mathbf{S}, \mathbf{P}) \cdot \\ & \quad p(\Theta | \mathbf{G}) p(\mathcal{D} | \mathbf{G}, \Theta) f(\mathbf{G}, \Theta) d\mathbf{Z} d\Theta \\ &= \int_{\Theta} \int_{\mathbf{Z}} \frac{p(\mathbf{Z})}{p(\mathcal{D})} \sum_{\mathbf{G}} \sum_{\mathbf{S}} p(\mathbf{G}, \mathbf{S} | \mathbf{Z}, \mathbf{P}) \cdot \\ & \quad p(\Theta | \mathbf{G}) p(\mathcal{D} | \mathbf{G}, \Theta) f(\mathbf{G}, \Theta) d\mathbf{Z} d\Theta \\ &= \int_{\Theta} \int_{\mathbf{Z}} \frac{p(\mathbf{Z})}{p(\mathcal{D})} \sum_{\mathbf{G}} p(\mathbf{G} | \mathbf{Z}, \mathbf{P}) \cdot \\ & \quad p(\Theta | \mathbf{G}) p(\mathcal{D} | \mathbf{G}, \Theta) f(\mathbf{G}, \Theta) d\mathbf{Z} d\Theta \\ &= \int_{\Theta} \int_{\mathbf{Z}} \frac{p(\mathbf{Z}, \Theta | \mathcal{D}, \mathbf{P})}{p(\mathcal{D}, \Theta | \mathbf{Z}, \mathbf{P})} \sum_{\mathbf{G}} p(\mathbf{G} | \mathbf{Z}, \mathbf{P}) \cdot \\ & \quad p(\Theta | \mathbf{G}) p(\mathcal{D} | \mathbf{G}, \Theta) f(\mathbf{G}, \Theta) d\mathbf{Z} d\Theta \\ &= \int_{\Theta} \int_{\mathbf{Z}} p(\mathbf{Z}, \Theta | \mathcal{D}, \mathbf{P}) \frac{1}{p(\mathcal{D}, \Theta | \mathbf{Z}, \mathbf{P})} \sum_{\mathbf{G}} p(\mathbf{G} | \mathbf{Z}, \mathbf{P}) \cdot \\ & \quad p(\Theta | \mathbf{G}) p(\mathcal{D} | \mathbf{G}, \Theta) f(\mathbf{G}, \Theta) d\mathbf{Z} d\Theta \\ &= \int_{\Theta} \int_{\mathbf{Z}} p(\mathbf{Z}, \Theta | \mathcal{D}, \mathbf{P}) \frac{1}{\sum_{\mathbf{G}} p(\mathcal{D}, \mathbf{G}, \Theta | \mathbf{Z}, \mathbf{P})}. \end{aligned}$$

$$\begin{aligned}
& \sum_{\mathbf{G}} p(\mathbf{G} | \mathbf{Z}, \mathbf{P}) p(\Theta | \mathbf{G}) \cdot \\
& \quad p(\mathcal{D} | \mathbf{G}, \Theta) f(\mathbf{G}, \Theta) d\mathbf{Z}d\Theta \\
= & \int_{\Theta} \int_{\mathbf{Z}} p(\mathbf{Z}, \Theta | \mathcal{D}, \mathbf{P}) \cdot \\
& \quad \frac{\sum_{\mathbf{G}} p(\mathbf{G} | \mathbf{Z}, \mathbf{P}) p(\Theta | \mathbf{G}) p(\mathcal{D} | \mathbf{G}, \Theta) f(\mathbf{G}, \Theta)}{\sum_{\mathbf{G}} p(\mathbf{G} | \mathbf{Z}, \mathbf{P}) p(\Theta | \mathbf{G}) p(\mathcal{D} | \mathbf{G}, \Theta)} \\
& \quad d\mathbf{Z}d\Theta \\
= & \int_{\Theta} \int_{\mathbf{Z}} p(\mathbf{Z}, \Theta | \mathcal{D}, \mathbf{P}) \cdot \\
& \quad \frac{\sum_{\mathbf{G}} p(\mathbf{G} | \mathbf{Z}, \mathbf{P}) p(\Theta, \mathcal{D} | \mathbf{G}) f(\mathbf{G}, \Theta)}{\sum_{\mathbf{G}} p(\mathbf{G} | \mathbf{Z}, \mathbf{P}) p(\Theta, \mathcal{D} | \mathbf{G})} d\mathbf{Z}d\Theta \\
= & \mathbb{E}_{p(\mathbf{Z}, \Theta | \mathcal{D}, \mathbf{P})} \left[\frac{\mathbb{E}_{p(\mathbf{G} | \mathbf{Z}, \mathbf{P})} [f(\mathbf{G}, \Theta) p(\Theta, \mathcal{D} | \mathbf{G})]}{\mathbb{E}_{p(\mathbf{G} | \mathbf{Z}, \mathbf{P})} [p(\Theta, \mathcal{D} | \mathbf{G})]} \right].
\end{aligned}$$

APPENDIX B

PROOF OF EQUATIONS (14) & (16)

Proof: The derivative of the posterior log likelihood $\log p(\mathbf{Z}, \Theta | \mathcal{D}, \mathbf{P})$ with respect to the latent variable \mathbf{Z} in Equation (14) is computed as

$$\begin{aligned}
& \nabla_{\mathbf{Z}} \log p(\mathbf{Z}, \Theta | \mathcal{D}, \mathbf{P}) \\
= & \nabla_{\mathbf{Z}} \log p(\mathbf{Z}, \Theta, \mathcal{D} | \mathbf{P}) - \nabla_{\mathbf{Z}} \log p(\mathcal{D} | \mathbf{P}) \\
= & \nabla_{\mathbf{Z}} \log p(\mathbf{Z}, \Theta, \mathcal{D} | \mathbf{P}) \quad (\text{as } \nabla_{\mathbf{Z}} \log p(\mathcal{D} | \mathbf{P}) = 0) \\
= & \nabla_{\mathbf{Z}} \log p(\mathbf{Z}) + \nabla_{\mathbf{Z}} \log p(\Theta, \mathcal{D} | \mathbf{Z}, \mathbf{P}) \\
= & \nabla_{\mathbf{Z}} \log p(\mathbf{Z}) + \frac{\nabla_{\mathbf{Z}} p(\Theta, \mathcal{D} | \mathbf{Z}, \mathbf{P})}{p(\Theta, \mathcal{D} | \mathbf{Z}, \mathbf{P})} \\
& \quad (\text{as } \nabla_{\mathbf{x}} \log g(\mathbf{x}) = \nabla_{\mathbf{x}} g(\mathbf{x}) / g(\mathbf{x})) \\
= & \nabla_{\mathbf{Z}} \log p(\mathbf{Z}) + \frac{\nabla_{\mathbf{Z}} [\sum_{\mathbf{G}} p(\mathbf{G}, \Theta, \mathcal{D} | \mathbf{Z}, \mathbf{P})]}{\sum_{\mathbf{G}} p(\mathbf{G}, \Theta, \mathcal{D} | \mathbf{Z}, \mathbf{P})} \\
= & \nabla_{\mathbf{Z}} \log p(\mathbf{Z}) + \frac{\nabla_{\mathbf{Z}} [\sum_{\mathbf{G}} p(\mathbf{G} | \mathbf{Z}, \mathbf{P}) p(\Theta, \mathcal{D} | \mathbf{G})]}{\sum_{\mathbf{G}} p(\mathbf{G} | \mathbf{Z}, \mathbf{P}) p(\Theta, \mathcal{D} | \mathbf{G})} \\
= & \nabla_{\mathbf{Z}} \log p(\mathbf{Z}) + \frac{\nabla_{\mathbf{Z}} \mathbb{E}_{p(\mathbf{G} | \mathbf{Z}, \mathbf{P})} [p(\Theta, \mathcal{D} | \mathbf{G})]}{\mathbb{E}_{p(\mathbf{G} | \mathbf{Z}, \mathbf{P})} [p(\Theta, \mathcal{D} | \mathbf{G})]}.
\end{aligned}$$

The derivative of the posterior log likelihood $\log p(\mathbf{Z}, \Theta | \mathcal{D}, \mathbf{P})$ with respect to the latent variable Θ in Equation (16) can also be computed easily by following these steps.

APPENDIX C

IMPLEMENTATION & HYPERPARAMETERS

TOBAC¹ is implemented using Python and the JAX [3] library. Our implementation is based on the implementation of DiBS [25]². For other approaches including BCD Nets [8]³ and DAG-GFlowNet [9]⁴, we use their original implementation for the experiments.

¹<https://github.com/quangdzuytran/TOBAC>

²<https://github.com/larslorch/dibs>

³<https://github.com/ermongroup/BCD-Nets>

⁴<https://github.com/tristandeleu/jax-dag-gflownet>

For synthesizing the data, we follow previous approaches [8], [25], [9] for data configurations. In the linear Gaussian synthetic data, the parameters θ_i of the edges are sampled from $\mathcal{N}(0, 1)$ with the additive noises sampled from $\mathcal{N}(0, 0.1)$. As in BCD Nets [8] and DiBS [25], a minimum value of 0.5 is applied to the parameters by adding $\text{sign}(\theta_i) \times 0.5$ to the sampled parameters to clarify whether the parent nodes have contributions in the variable. This value is also chosen as the threshold for determining if an edge exists in BCD Nets. In nonlinear Gaussian data, the data is generated from neural networks with one hidden layer comprising of 5 nodes and ReLU activation. The parameters in the neural networks are also sampled from $\mathcal{N}(0, 1)$ with observation noises sampled from $\mathcal{N}(0, 0.1)$ as in the linear Gaussian setting. These configurations are also applied to the corresponding inference models. In the experiments with the flow cytometry dataset [36], the linear Gaussian model is chosen for inferring the probability of the parameters given the graph.

The ground-truth topological orderings in the experiments are obtained from the ground-truth DAGs using the topological sorting algorithm [29] of the NetworkX [16] library. In order to use EqVar [5]⁵ and NPVar [14]⁶ for finding the orderings, we re-implement these methods with NumPy [17] and pyGAM [38] from their R implementations. Regarding SCORE [35]⁷, as the PyTorch [33] version of the code is available, we utilize their original implementation.

All of the baselines are also implemented with the JAX library. Our experiments with TOBAC and DiBS are performed with the hyperparameters in Table II, which are chosen in accordance to a similar approach of DiBS [25].

TABLE II
CHOSEN HYPERPARAMETERS FOR TOBAC IN THE EXPERIMENTS

Hyperparameter	Description	Value
M	Number of particles in Stein variational gradient descent	30
$\tilde{\alpha}$	The linear rate of $\alpha_t := \tilde{\alpha}t$	0.05
$(\gamma_z, \gamma_\theta)$	Bandwidths of the kernel	(5, 500)
σ_z	Standard deviation of latent variable \mathbf{Z}	$1/\sqrt{k}$
σ_{obs}	Standard deviation of observation noise	0.1
η_{t_0}	Initial learning rate of RMSProp	0.005
(μ_e, σ_e)	Mean and standard deviation of the parameters in linear Gaussian models	(0, 1)
σ_p	Standard deviation of the parameters in nonlinear Gaussian models	1
L	Number of hidden layers in nonlinear Gaussian models	5

⁵<https://github.com/WY-Chen/EqVarDAG>

⁶<https://github.com/MingGao97/NPVAR>

⁷<https://github.com/paulrolland1307/SCORE>